Article

Free-Standing Nanocomposite Multilayers with Various Length Scales, Adjustable Internal Structures, and Functionalities

Seryun Lee, Bokyoung Lee, Bumjoon J. Kim, Junwoo Park, Misang Yoo, Wan Ki Bae, Kookheon Char, Craig J. Hawker, Joona Bang, and Jinhan Cho

J. Am. Chem. Soc., **2009**, 131 (7), 2579-2587• Publication Date (Web): 30 January 2009

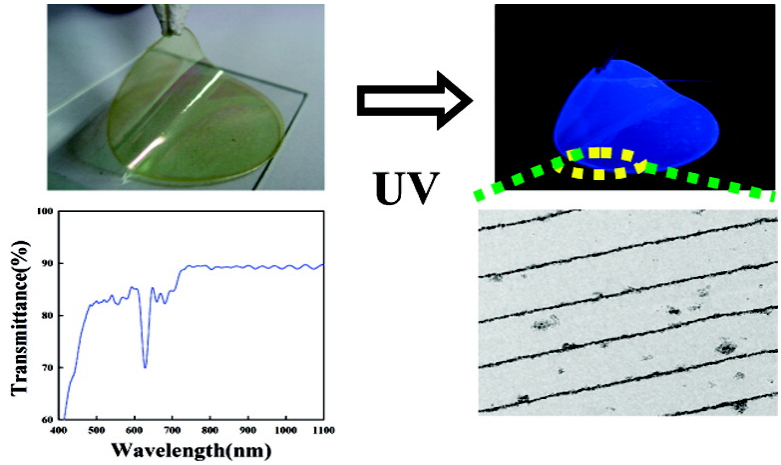

More About This Article

Additional resources and features associated with this article are available within the HTML version:

- Supporting Information
- Access to high resolution figures
- Links to articles and content related to this article
- Copyright permission to reproduce figures and/or text from this article

View the Full Text HTML

J|A|C|S ARTICLES

Published on Web 01/30/2009

Free-Standing Nanocomposite Multilayers with Various Length Scales, Adjustable Internal Structures, and Functionalities

Seryun Lee,[†] Bokyoung Lee,[†] Bumjoon J. Kim,[‡] Junwoo Park,[§] Misang Yoo,[§] Wan Ki Bae,[||] Kookheon Char,[||] Craig J. Hawker,[⊥] Joona Bang,*[,§] and Jinhan Cho*[,†]

School of Advanced Materials Engineering, Kookmin University, Jeongneung-dong, Seongbuk-gu, Seoul 136-702, Korea, Department of Chemical and Biomolecular Engineering, Korea Advanced Institute of Science and Technology, Daejeon 305-701, Korea, Department of Chemical and Biological Engineering, Korea University, Anam-dong, Seongbuk-gu, Seoul 136-701, Korea, School of Chemical and Biological Engineering, Seoul National University, San 56-1, Shinlim-dong, Kwanak-gu, Seoul 151-744, Korea, and Materials Research Laboratory, University of California, Santa Barbara, California 93106-5121

Received August 20, 2008; E-mail: jinhan@kookmin.ac.kr; joona@korea.ac.kr

Abstract: We introduce an innovative and robust method for the preparation of nanocomposite multilayers, which allows accurate control over the placement of functional groups as well as the composition and dimensions of individual layers/internal structure. By employing the photocross-linkable polystyrene (PS−N_3, M_n = 28.0 kg/mol) with 10 wt % azide groups (−N_3) for host polymer and/or the PS−N_3−SH (M_n = 6.5 kg/mol) with azide and thiol (−SH) groups for capping ligands of inorganic nanoparticles, nanocomposite multilayers were prepared by an efficient photocross-linking layer-by-layer process, without perturbing underlying layers and nanostructures. The thickness of individual layers could be controlled from a few to hundreds of nanometers producing highly ordered internal structure, and the resulting nanocomposite multilayers, consisting of polymer and inorganic nanoparticles (CdSe@ZnS, Au, and Pt), exhibit a variety of interesting physical properties. These include prolonged photoluminescent durability, facile color tuning, and the ability to prepare functional free-standing films that can have the one-dimensional photonic band gap and furthermore be patterned by photolithography. This robust and tailored method opens a new route for the design of functional film devices based on nanocomposite multilayers.

Introduction

Nanocomposite multilayer films, which can be prepared by the self-assembly of block copolymers,[1] molecular recognition approach,[2,3] or layer-by-layer (LbL) assembly methods,[4] have attracted considerable attention recently. This is driven by the ability to easily process the polymeric films coupled with an ability to disperse functional nanostructures in these films, which leads to a range of potential applications. In turn these applications are strongly dependent on individual layer thickness and internal structures as well as the nature of the dispersed inorganic/metallic components.[5−11] For multilayers with thicknesses ranging from tens to hundreds of nanometers, the films can be used for nonvolatile memory devices, light emitting diodes, electrochemical sensors, and antireflective films.[8−11] For thicker multilayers with layer thicknesses of hundreds of nanometers, mechanically reinforced films have been prepared and exploited.[5−7] Given the wide interest and range of potential applications for these nanocomposite multilayers, it is critical to develop general synthetic and process strategies that allow a high degree of control over film/layer dimensions (from the angstrom level to hundreds of nanometers) and flexible free-standing films while at the same time permitting the incorporation and controlled dispersion of a wide variety of functional components.

For the fabrication of multilayer structures, it has been demonstrated that the LbL assembly method is potentially the most versatile and offers the opportunity to prepare nanocom-

[†] Kookmin University.
[‡] Korea Advanced Institute of Science and Technology.
[§] Korea University.
[||] Seoul National University.
[⊥] University of California.

(1) Kim, B. J.; Bang, J.; Hawker, C. J.; Chiu, J. J.; Pine, D. J.; Jang, S. G.; Yang, S.-M.; Kramer, E. J. *Langmuir* **2007**, *23*, 12693–12703.
(2) Boal, A. K.; Ilhan, F.; DeRouchey, J. E.; Thurn-Albrecht, T.; Russell, T. P.; Rotello, V. M. *Nature* **2000**, *404*, 746–748.
(3) Uzun, O.; Frankamp, B. L.; Sanyal, A.; Rotello, V. M. *Chem. Mater.* **2006**, *18*, 5404–5409.
(4) Decher, G. *Science* **1997**, *277*, 1232–1237.
(5) Podsiadlo, P.; Kaushik, A. K.; Arruda, E. M.; Waas, A. M.; Shim, B. S.; Xu, J. D.; Nandivada, H.; Pumplin, B. G.; Lahann, J.; Ramamoorthy, A.; Kotov, N. A. *Science* **2007**, *318*, 80–83.
(6) Tang, Z. Y.; Kotov, N. A.; Magonov, S.; Ozturk, B. *Nat. Mater.* **2003**, *2*, 413–418.
(7) Wang, T. C.; Cohen, R. E.; Rubner, M. F. *Adv. Mater.* **2002**, *14*, 1534–1537.
(8) Lee, J. S.; Cho, J.; Lee, C.; Kim, I.; Park, J.; Kim, Y. M.; Shin, H.; Lee, J.; Caruso, F. *Nat. Nanotechnol.* **2007**, *2*, 790–795.
(9) Ho, P. K. H.; Kim, J. S.; Burroughes, J. H.; Becker, H.; Li, S. F. Y.; Brown, T. M.; Cacialli, F.; Friend, R. H. *Nature* **2000**, *404*, 481–484.
(10) Yu, A. M.; Liang, Z. J.; Cho, J. H.; Caruso, F. *Nano Lett.* **2003**, *3*, 1203–1207.
(11) Cho, J. H.; Hong, J. K.; Char, K.; Caruso, F. *J. Am. Chem. Soc.* **2006**, *128*, 9935–9942.

posite films with tailored electrical, mechanical, or optical properties. An important advantage of this method is that it enables the preparation of films with controlled thickness, composition, and functionality through complementary interactions (i.e., electrostatic,[4,12] hydrogen-bonding,[5,13−15] or covalent interaction[16]). However, a disadvantage of the conventional LbL method based on dip[5−13] or spin-coating[17−19] is in terms of efficiency, especially for thicker films as layer deposition requires adsorption of the desired materials via a self- or forced diffusion process followed by rinsing of weakly adsorbed materials. For example, for the fabrication of functional multilayer films with micron-scale thickness, these films should have hundreds of layers (i.e., hundreds of deposition cycles) because each deposition process adds up to only a few nanometers thick layer after rinsing. Furthermore, the conventional LbL approach cannot be applied for the buildup of multilayers containing nonpolar or uncharged polymers and nanoparticles. In addition, it is not possible to easily incorporate layers of differing chemistry of hydrophilic/hydrophobic balance in the traditional LbL process.[20] Resultantly, this assembly has much difficulty in the preparation of various functional free-standing multilayers with micron-scale thickness and hydrophobic properties due to the disadvantages as mentioned above.

Herein, we introduce a novel strategy for the preparation of free-standing nanocomposite multilayers with various length scales, functionalities, and adjustable internal structures. The strategy is based on the use of hydrophobic polymers containing UV cross-linkable units and/or high affinity groups with the polymers and/or polymer-coated nanoparticles being consecutively deposited by spin-coating. The photocross-linking of each layer allows various thicknesses to be achieved without any rinsing or intermediate purification steps. When optically active nanoparticles such as QDs are incorporated into the photocross-linkable polymer layers, the photoluminescent durability is significantly enhanced while also allowing facile color tuning. Remarkably, we show that the internal structure of multilayer films can be controlled via segregation between polymer-coated nanoparticles and polymers during the spin-coating step. Furthermore, it is demonstrated that this novel strategy can be extended to the functional free-standing multilayers through use of sacrificial ionic substrates (NaCl) and adjustment of internal structures or photopatterning. We highlight that our photocross-linking LbL assembly is a simpler and more versatile process for the fabrication of functional nanocomposite multilayers including free-standing films than any other method introduced to date. Therefore, we strongly believe that our approach can provide the basis for the preparation of many potential applications such as highly flexible optical and electronic devices.

Experimental Section

Materials. Photocross-linkable polymers, PS−N_3 (M_n = 28.0 kg/mol) and PS−N_3−SH (M_n = 6.5 kg/mol), were synthesized via reversible addition fragmentation transfer (RAFT) polymerization.[21] For PS−N_3, styrene (5.0 g, 0.048 mol), 4-vinylbenzyl chloride (0.5 g, 3.33 mmol), 2,2′-azobis(2-methylpropionitrile) (AIBN) (2 mg, 0.014 mmol), and RAFT agent (27 mg, 0.09 mmol) were mixed and degassed. The reaction was carried out at 70 °C for 48 h. The reaction mixture was then precipitated into methanol, resulting in the random copolymer as a pink powder. To avoid the coupling during the azidation, the dithioester end group was removed by the reaction with AIBN under nitrogen (80 °C for 12 h). The solution was precipitated into methanol, obtaining the white powder. The change in color suggested that the dithioester group was removed. Then, the polymer was stirred with 3 equivalents of sodium azide in dimethylformamide at the ambient condition for 12 h. The solution was filtered and precipitated into methanol to give a final product, PS−N_3, as a white powder. From size exclusion chromatography (SEC), the M_n and PDI were 28.0 kg/mol and 1.1, respectively. The composition of the azide group in PS−N_3 was found to be 0.10 from proton NMR. The thiol-terminated random copolymer, PS−N_3−SH, was synthesized by the similar procedure as PS−N_3. The only difference is the reaction with AIBN was replaced by the reaction with hexylamine to convert the dithioester group to the thiol group. The detailed procedure regarding this reaction is described in ref 1. The M_n and PDI were 6.5 kg/mol and 1.1, respectively. The composition of the azide group in PS−N_3−SH was 0.10.

Oleic acid-stabilized CdSe@ZnS with green and red emissive colors was synthesized as previously reported.[22] It was reported that high quality QDs can be easily synthesized using oleic acid stabilizers.[23] For blue emissive QDs, 38.5 mg of CdO, 700 mg of zinc acetate, 17.6 mL of oleic acid, and 15 mL of 1-octadecene were put into a 250 mL round flask. The mixture was heated to 150 °C with N_2 gas blowing and further heated to 300 °C to form a clear solution of $Cd(OA)_2$ and $Zn(OA)_2$. At this temperature, 31 mg of Se powder and 128.2 mg of S powder both dissolved in 2 mL of trioctylphosphine were quickly injected into the reaction flask. After the injection, the temperature of the reaction flask was set to 300 °C for promoting the growth of QDs, and it was then cooled to room temperature to stop the growth. QDs were purified by adding 20 mL of chloroform and an excess amount of acetone (3 times). After this purification, PS−N_3−SH of 2 wt % was added to a QD solution of 15 mL for the stabilizer exchange from oleic acid to N_3−PS−SH and then was heated at 40 °C for 2 h.

Water-soluble Au or Pt nanoparticles (Au_{NP} or Pt_{NP}) were synthesized as reported in our previous papers.[8,24] Briefly, 250 mL of 1.79 mM $HAuCl_4$ or $H_2Cl_6Pt\cdot 6H_2O$ was maintained at room temperature with vigorous stirring. Rapid addition of 20 mL of 68 mM sodium citrate to the vortex of the solution and successive addition (1 mL) of 70 mM $NaBH_4$ resulted in a color change from dark yellow to dark brown. The diameters of synthesized Au_{NP} and Pt_{NP} were about 8 and 6 nm, respectively, as confirmed by TEM images. These nanoparticles were dispersed in aqueous solution at pH 5. The Au_{NP} or Pt_{NP} solution of about 20 mL was mixed with PS−N_3−SH toluene solution of about 7 mL for phase transfer of Au_{NP} or Pt_{NP} from water to toluene phase. In this case, metal nanoparticles dispersed in toluene were highly concentrated.

(12) Caruso, F.; Caruso, R. A.; Möhwald, H. *Science* **1998**, *282*, 1111–1114.
(13) Lutkenhaus, J. L.; Hrabak, K. D.; McEnnis, K.; Hammond, P. T. *J. Am. Chem. Soc.* **2005**, *127*, 17228–17234.
(14) Cho, J.; Caruso, F. *Macromolecules* **2003**, *36*, 2845–2851.
(15) Girolamo, J. D.; Reiss, P.; Pron, A. *J. Phys. Chem. C* **2008**, *112*, 8797–8801.
(16) Such, G. K.; Quinn, J. F.; Quinn, A.; Tjipto, E.; Caruso, F. *J. Am. Chem. Soc.* **2006**, *128*, 9318–9319.
(17) Cho, J.; Char, K.; Hong, J. D.; Lee, K. B. *Adv. Mater.* **2001**, *13*, 1076–1078.
(18) Cho, J.; Char, K. *Langmuir* **2004**, *20*, 4011–4016.
(19) Chiarelli, P. A.; Johal, M. S.; Casson, J. L.; Roberts, J. B.; Robinson, J. M.; Wang, H. L. *Adv. Mater.* **2001**, *13*, 1167–1171.
(20) Krishnan, R. S.; Mackay, M. E.; Duxbury, P. M.; Pastor, A.; Hawker, C. J.; Van Horn, B.; Asokan, S.; Wong, M. S. *Nano Lett.* **2007**, *7*, 484–489.
(21) Bang, J.; Bae, J.; Lowenhielm, P.; Spiessberger, C.; Given-Beck, S. A.; Russell, T. P.; Hawker, C. J. *Adv. Mater.* **2007**, *19*, 4552–4557.
(22) Bae, W. K.; Char, K.; Hur, H.; Lee, S. *Chem. Mater.* **2008**, *20*, 531–539.
(23) Yu, W. W.; Peng, X. *Angew. Chem., Int. Ed. Engl.* **2002**, *41*, 2368–2371.
(24) Park, J.; Kim, I.; Shin, H.; Lee, M. J.; Kim, Y. S.; Bang, J.; Caruso, F.; Cho, J. *Adv. Mater.* **2008**, *20*, 1843–1848.

Buildup of Multilayers. The concentration of PS−N_3 solutions was controlled from 0.1 to 5 wt %. For the spin-assembled multilayer films, PS−N_3 solution or blending solution of PS−N_3 (2 wt %) and PS−N_3−SH−QD (2 wt %) was completely wetted on the quartz or silicon substrates. The substrate was then rotated with a spinner at 3000 rpm for 20 s, and the resulting films were photocross-linked under UV irradiation ($\lambda = 254$ nm) for 60 s. The next layers were also sequentially deposited onto the previous films using the same procedure. These processes were repeated up to desired deposition cycles. In the case of free-standing films, the multilayers were sequentially deposited onto NaCl substrates with repetitive UV irradiation and then dipped into the water bath to dissolve the substrates.

Measurements. UV−vis spectra were taken with a Perkin−Elmer Lambda 35 UV−vis spectrometer. The benzene ring with azide groups of PS−N_3 has an absorbance peak centered at 255 nm. PL spectra were taken with a fluorescence spectrometer (Perkin−Elmer LS 55). The PL spectra of PS-encapsulated multilayers were measured at an excitation wavelength of $\lambda_{ex} \approx 400$ nm. FTIR spectra were taken with a FTIR-200 spectrometer (JASCO Corporation). PS−N_3 single layer was spin-cast onto CdSe crystal substrates at 1000 rpm. The FTIR absorption peaks of azide (−N_3) groups occurring at 2100 cm^{-1} were investigated with increasing UV irradiation time. The decomposed amount of azide groups is equivalent to those taking part in PS−N_3 cross-linking.

A QCM device (QCM200, SRS) was used to investigate the mass of material deposited after each adsorption step. The resonance frequency of the QCM electrodes was ca. 5 MHz. The adsorbed mass of PS−N_3−SH and Au_{NP}, Δm, can be calculated from the change in QCM frequency, ΔF, according to the Sauerbrey equation:[25] ΔF (Hz) $= -56.6 \times \Delta m_A$, where Δm_A is the mass change per quartz crystal unit area, in $\mu g \cdot cm^{-2}$. The thicknesses and refractive indices of the PS−N_3 multilayer films on Si wafers were measured by ellipsometry (Gaertner Scientific Corp., L2W15S830) with 632.8 nm He−Ne laser light. The total thicknesses of PS-encapsulated multilayer films were measured from FE-SEM tilted images (i.e., the total thicknesses were compensated for the tilt angle of 10°).

Results and Discussion

In developing robust, photocross-linkable materials, our attention was directed toward random copolymers of styrene and *p*-azidomethylstyrene due to the chemical stability of the azide group, facile synthesis from chloromethylstyrene units, and its direct photocross-linking reaction.[21] As a result, random copolymers carrying the UV-sensitive azide group, denoted PS−N_3, were used as the matrix polymer (Figure 1a), and thiol-terminated random copolymers, denoted PS−N_3−SH, were used as a UV cross-linkable stabilizer of CdSe@ZnS (i.e., CdSe core with ZnS shell), Au, and Pt nanoparticles (Figure 1b). In this case, UV irradiation of the azide groups in the polymer backbone leads to the formation of highly reactive nitrene radicals, which undergo facile cross-linking in the absence of additional additives. Based on these photocross-linking reactions, the PS−N_3 multilayers can be prepared by a repetitive process of spin-coating and UV cross-linking without the necessity for complementary interactions or backbone compatibility (Figure 2a). It should be noted that these azide groups could be easily introduced into various polymers (see Experimental Section).

The cross-linking reaction by photodissociation of azide groups was confirmed by disappearance of the absorbance peak at 2100 cm^{-1} for the azide groups in the FTIR. UV irradiation for 50 s resulted in approximately 70% reaction within the spin-coated PS−N_3 films and leads to formation of a stable, cross-linked layer which is not removed by toluene washing (Figure 2b). The thickness of the individual layer can be readily adjusted according to the polymer concentration and spinning speed. First, we investigated the vertical growth of cross-linked multilayers (0.1 wt % solution concentrations) through consecutive spin-coating and photocross-linking (Figure 2c). The absorbance at 255 nm originates from the phenyl rings of the polystyrene backbone, and the uniform growth of this peak suggests that the fabrication process is controlled leading to regular, multilayer growth. It should be noted that the respective layer thickness can be significantly increased by increasing solution concentration or reducing spinning speed, and this degree of versatility is significantly greater than the recently reported synthesis of covalent LbL multilayers by copper-catalyzed click chemistry.[16] For example, increasing the solution concentration from 0.1 to 4 wt % increases the respective layer thickness from 1.6 to about 150 nm with uniform layer growth (Figure 2d).

The mechanical properties of PS−N_3 ($M_n = 28.0$ kg/mol) and pure PS ($M_n = 26.0$ kg/mol) films have been measured using depth-sensing indentation experiments. It was found that the elastic modulus of PS−N_3 and PS films with 200 nm thicknesses was measured to be 4.525 ± 0.220 and 4.348 ± 0.395 GPa, respectively. Additionally, the hardness of PS−N_3 and PS was measured to be 0.612 ± 0.035 and 0.513 ± 0.050 GPa, respectively. These similar mechanical properties were also supported by the fact that there was no significant difference in glass transition temperature between PS−N_3 (101 °C) and PS films (100.5 °C).

Based on these results, optically tunable organic−inorganic multilayers were prepared using a mixture of PS−N_3−SH-encapsulated QD nanoparticles (PS−N_3−SH−QD) and PS−N_3 polymers. Initially, oleic acid-stabilized CdSe@ZnS nanoparticles ranging from blue to red emissive colors were synthesized (see Supporting Information, Figure S1) and then ligand-exchanged with the reactive PS−N_3−SH stabilizers (see Supporting Information, Figure S2). After the ligand-exchange step, we found that most of the oleic acid was successfully exchanged to PS−N_3−SH, as the residual amount of oleic acid in PS−N_3−SH−QDs was measured to be less than 5 mol % by nuclear magnetic resonance (NMR) spectroscopy (see Supporting Information, Figure S3). In this case, PS−N_3−SH−QDs are well dispersed with the matrix polymer, PS−N_3, due to the favorable interactions between PS−N_3−SH and PS−N_3. From these dispersed films, nanocomposite (PS−N_3−SH−QDs: PS−N_3)$_n$ multilayers comprising PS−N_3−SH−QDs and PS−N_3 could be prepared as described above. The critical importance of the reactive ligands for the nanoparticles was demonstrated by the use of PS−SH-encapsulated QDs that do not contain photocross-linkable groups. In this case the nanoparticles were removed from the film during deposition of the next layer despite UV cross-linking of the matrix polymer (i.e., PS−N_3). Introduction of cross-linkable groups to the surface of the nanoparticles and covalent stabilization within the matrix is therefore critical for the preparation of well-defined organic−inorganic multilayer composites.

An additional benefit of the covalent stabilization is that the quenching effect of photoluminescence shown in water-soluble stabilizer-encapsulated QDs is significantly suppressed. In the case of traditional LbL-assembled QD multilayers,[26,27] solution

(25) Buttry, D. *Advances in electroanalytical chemistry: Applications of the QCM to electrochemistry*; Marcel Dekker: New York, 1991.
(26) Yang, P.; Li, C. L.; Murase, N. *Langmuir* **2005**, *21*, 8913–8917.
(27) Jaffar, S.; Nam, K. T.; Khademhosseini, A.; Xing, J.; Langer, R. S.; Belcher, A. M. *Nano Lett.* **2004**, *4*, 1421–1425.

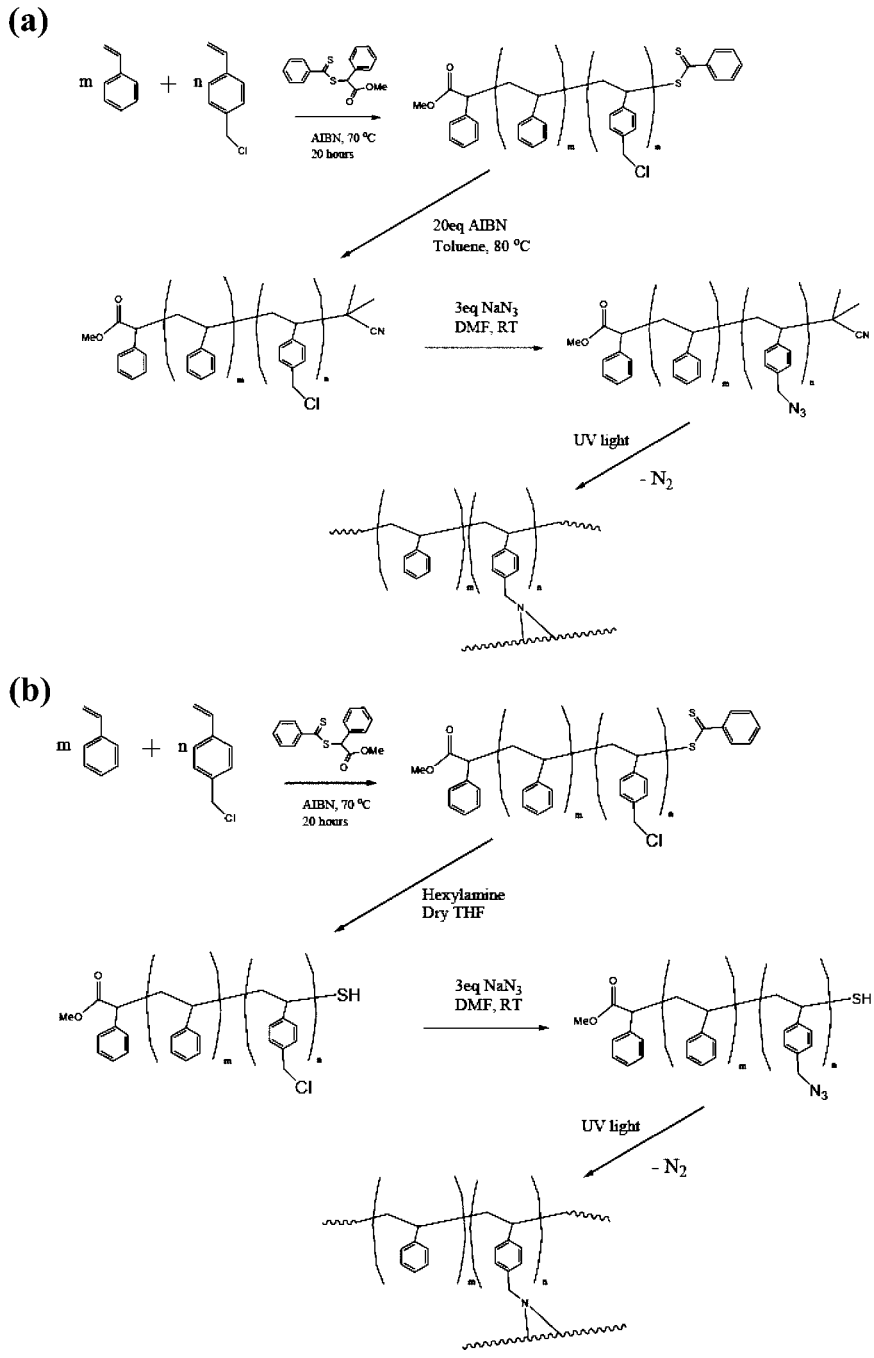

Figure 1. Schematics for the synthesis of photocross-linkable polymers: (a) PS−N_3 and (b) PS−N_3−SH. These polymers contain 10 mol % of azide group. These materials were synthesized via living free-radical polymerization (RAFT) from styerene and *p*-chloromethylstyrene followed by nucleophilic displacement with sodium azide and end group modification.

pH, nature of the hydrophilic ligands, extent of ligand exchange, and size of ligand groups all play a significant role in solution stability and quantum yield of QDs.[28−31] However, the QDs encapsulated by bulky cross-linkable PS (i.e., M_w of PS−N_3−SH ∼ 6.5 kg/mol) are highly luminescent (i.e., relative quantum yield of about 80∼90% in comparison with that of oleic acid-stabilized QDs), and Figure 3a displays the PL spectra and photographic images of (PS−N_3−SH−QDs:PS−N_3)$_3$ multilayers measured at an excitation wavelength of 365 nm. The fluorescence from three different kinds of QDs were adjusted to blue (λ_{max} ∼ 470 nm for PL maximum peak and QD diameter (D) ≈ 4.5 nm), green (λ_{max} ≈ 520 nm and D ≈ 5.0 nm), and red (λ_{max} ≈ 610 nm and D ≈ 5.4 nm) through size control of QDs, respectively. The concentration of QDs, PS−N_3−SH, and PS−N_3 was 1, 2, and 2 wt %, respectively, and the thickness of individual layer was about 109 nm. Even after deposition of three layers, the films were observed to emit fluorescent light that is clearly detectible with the naked eye under irradiation

(28) Medintz, I. L.; Uyeda, H. T.; Goldman, E. R.; Mattoussi, H. *Nat. Mater.* **2005**, *4*, 435–446.
(29) Hering, V. R.; Gibson, G.; Schumacher, R. I.; Faljoni-Alario, A.; Politi, M. J. *Bioconjugate Chem.* **2007**, *18*, 1705–1708.
(30) Mattoussi, H.; Mauro, J. M.; Goldman, E. R.; Anderson, G. P.; Sundar, V. C.; Mikulec, F. V.; Bawendi, M. G. *J. Am. Chem. Soc.* **2000**, *122*, 12142–12150.
(31) Hong, J.; Bae, W. K.; Lee, H.; Oh, S.; Char, K.; Caruso, F.; Cho, J. *Adv. Mater.* **2007**, *19*, 4364–4369.

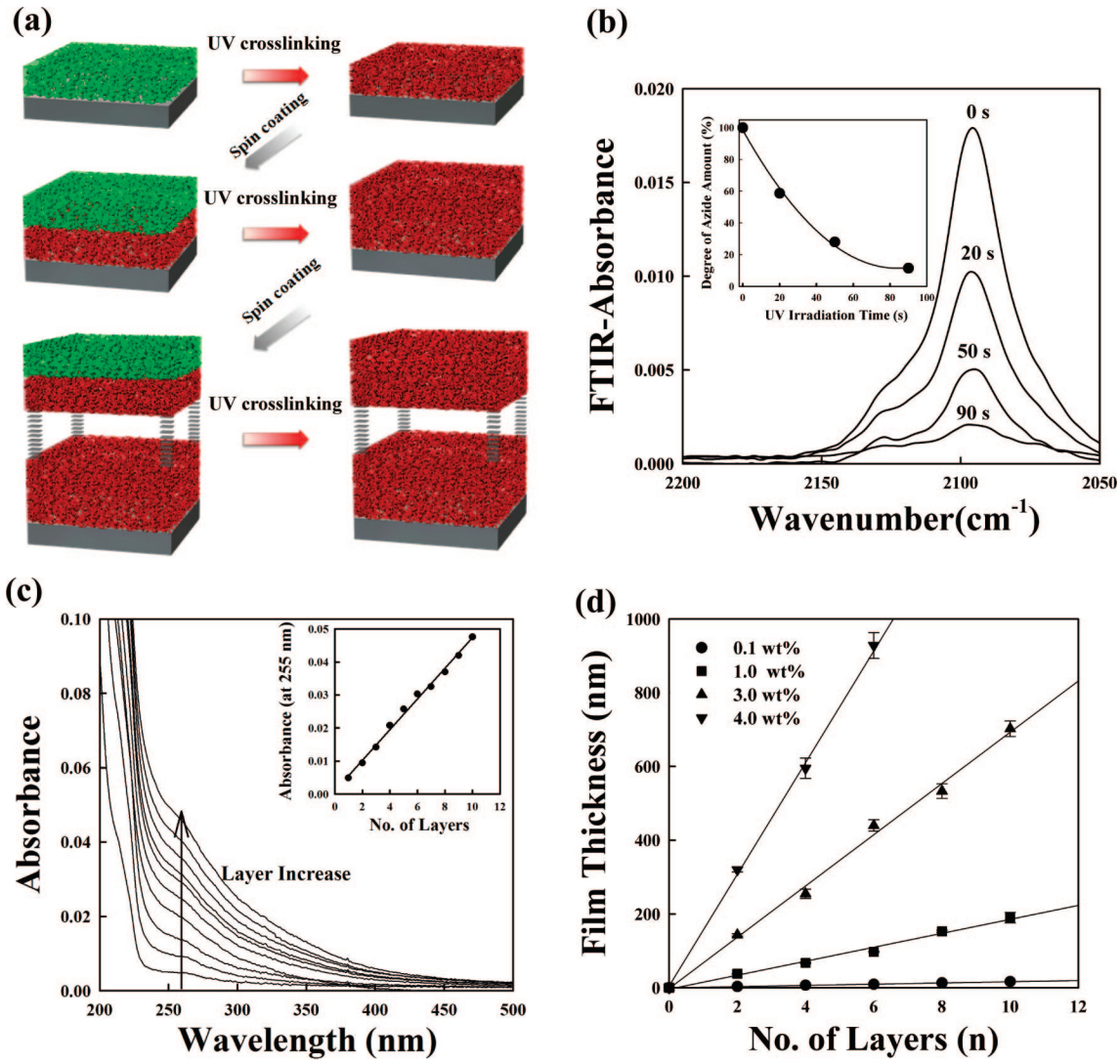

Figure 2. (a) Schematic for buildup of multilayers based on photocross-linkable PS. (b) FTIR absorption spectra of UV cross-linkable PS (single layer prepared from PS solution of 3 wt %) containing azide groups of 10 mol %. Azide absorption peak at 2095 cm^{-1} decreases with increasing irradiation time under UV irradiation of 254 nm. The inset shows the decomposed amount of azide groups as a function of irradiation time calculating the area of FTIR absorption peaks. (c) UV−vis absorption spectra of $(PS-N_3)_n$ measured with increasing the layer number (n) from 1 to 10. In this case the concentration of $PS-N_3$ was adjusted to 0.1 wt %. The inset shows the linear increase of absorbance measured at 255 nm wavelength as a function of layer number. (d) Change in the thickness of $(PS-N_3)_n$ multilayers prepared from three different kinds of solution concentration as a function of layer number (n). In this case, the thicknesses per layer are measured to be about 1.66 nm for 0.1 wt %, 19.0 nm for 1 wt %, 70.2 nm for 3 wt %, and 109 nm for 4 wt % concentrations, respectively.

of a low-power hand-held UV lamp. As a result, the fluorescent intensity can be easily manipulated by optimizing the deposition cycles (Figure 3b) or the QDs concentration (or number density of QDs). The number density of inserted green QDs within single layer (Figure 3b) was measured to be about 1.4×10^{13}/cm^2 (the frequency difference of quartz crystal microbalance between $PS-N_3-SH-$QDs and pure $PS-N_3-SH$ layer is about 250 Hz (i.e., 4.43 $\mu g/cm^2$). Also, the density of CdSe and ZnS is about 5.81 and 3.89 g/cm^3, respectively. Therefore, the number density of QDs can be roughly calculated based on the size of CdSe@ZnS (about 5 nm) and CdSe core (about 4 nm)[32−34] for green color, frequency change, and density of CdSe and ZnS). This approach is very simple and efficient when compared to conventional LbL methods based on complementary interaction, which is complicated by a strong quenching effect and the solution stability (i.e., the small ligands with thiol and carboxylic acid groups or the control of solution pH).

The advantages of this spin-coating strategy were exploited in the fabrication of white color emissive films which were prepared as schematically shown in Figure 3c. Since partial overlap between the PL spectrum of blue emitting QDs and the absorption spectra of green emitting QDs can induce fluorescence resonance energy transfer (FRET) at the interface of these layers, we designed multilayer structures with a deposition order of blue (one layer), red (three layers), and then green (two layers) emissive layers. From this complex, yet easy to prepare multilayer composite nanostructure, white light with a broad spectral emission was observed, showing the three

(32) Murray, C. B.; Norris, D. J.; Bawendi, M. G. *J. Am. Chem. Soc.* **1993**, *115*, 8706–8715.
(33) Wang, Q. B.; Seo, D. K. *Chem. Mater.* **2006**, *18*, 5764–5767.
(34) Rogach, A. L.; Kornowski, A.; Gao, M. Y.; Eychmuller, A.; Weller, H. *J. Phys. Chem. B* **1999**, *103*, 3065–3069.
(35) Templeton, A. C.; Wuelfing, M. P.; Murray, R. W. *Acc. Chem. Res.* **2000**, *33*, 27–36.

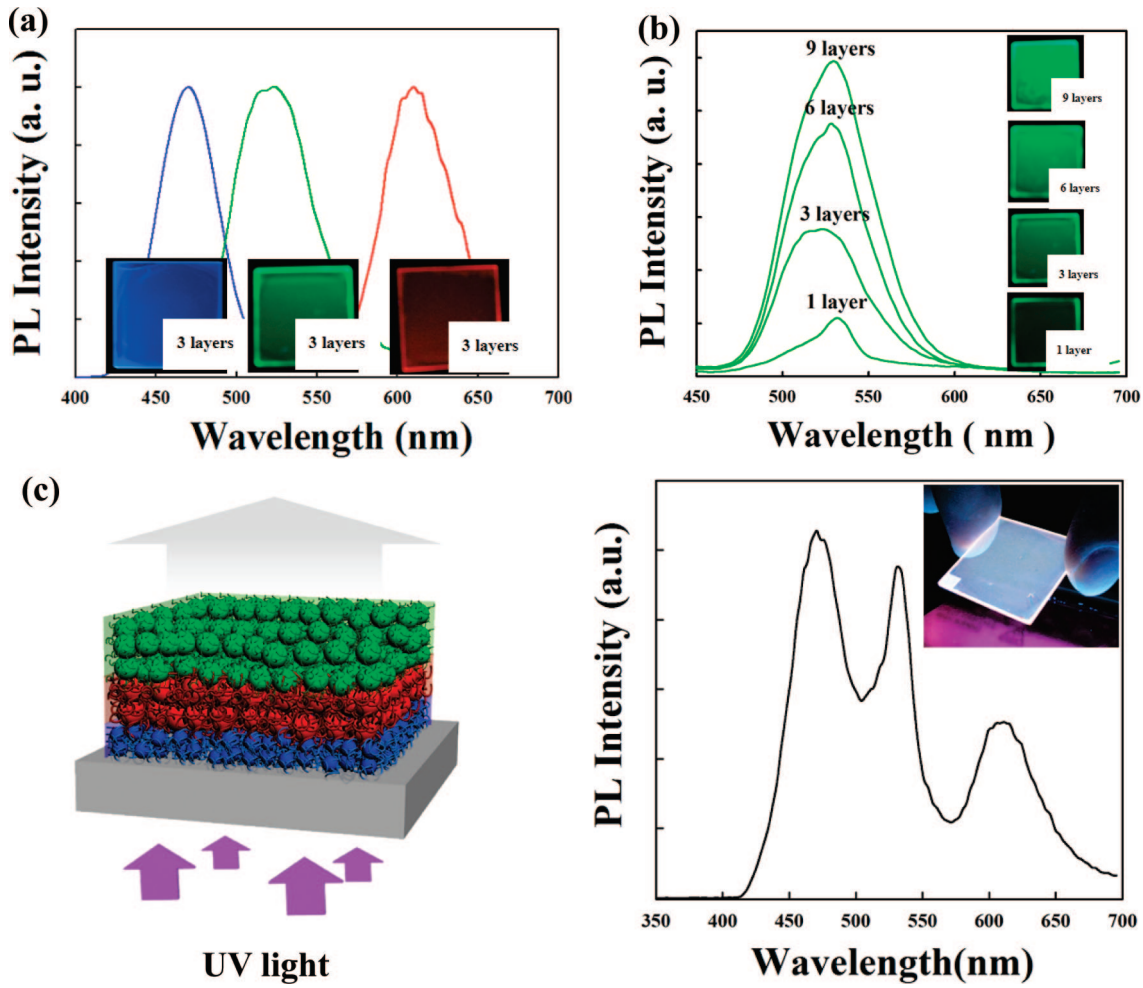

Figure 3. (a) PL spectra and photographic images of $(PS-N_3{:}PS-N_3-SH-QDs)_3$ multilayers prepared from blue, green, and red emitting QDs. The used solution concentrations of $PS-N_3$ and $SH-PS-N_3$ are all adjusted to 2 wt %. The excitation wavelengths for PL and photographic images are 400 and 365 nm, respectively. (b) PL spectra and photographic images of $(PS-N_3{:}PS-N_3-SH-\text{green QDs})_n$ with increasing layer number (n) from 1 to 9. The used solution concentrations of UV cross-linkable PS and the excitation wavelength were the same as those of (a). (c) Schematic, PL spectrum, and photographic image for white color emissive multilayer films. The blue (one layer), red (three layers), and green emissive layers (two layers) were deposited onto quartz glass in order.

different PL peaks pertaining to blue, green, and red spectral components. As mentioned earlier, the fluorescence intensity of these films can be significantly increased by increasing the number of deposition cycles or the QD concentration. A key feature of this work is the ability to prepare white fluorescent QD multilayers with sufficient intensity to be detectible by the naked eye, which is in contrast to other reports of white color emission generated by electroluminescence from a mixed monolayer of red, green, and blue emitting QDs which due to the low fluorescent intensity cannot be seen.

Furthermore, polymer-coated QD multilayers were deposited onto sacrificial ionic substrates (NaCl) in order to fabricate free-standing multilayer films with highly luminescent properties. By dissolving the NaCl substrate in water, hydrophobic PS−QD multilayers could be easily obtained, and this simple method allowed free-standing and transparent $(PS-N_3-SH-QD{:}PS-N_3)_n$ multilayers with controlled thickness, optical property, and light transmission of ca. 90% to be obtained (Figure 4a). The size of detached free-standing films is only limited to the substrate size, and this can be further scalable. Deposition layer number (n) for the preparation of free-standing $(PS-N_3-SH-QD{:}PS-N_3)_n$ multilayers could be decreased to 10 layers allowing the facile control of film flexibility (Figure 4b). Additionally, these films could be stored under ambient conditions for 2+ months and were shown to maintain their highly luminescent properties without any decrease in PL intensity. Conceivably the hydrophobic and covalently cross-linked environment of the nanoparticles protects them from oxidative damage and moisture-induced PL quenching (see Supporting Information, Figure S4).

Another remarkable feature is that the internal structure of free-standing multilayers is highly ordered as shown by the cross-sectional transmission electron microscopy (TEM) image in Figure 4a. Simple spin-coating can lead to two distinct layers composed of $PS-N_3-SH-QD$ and $PS-N_3$ layers (more details are given below). Cross-linking followed by repeated spin-coating stabilizes this self-assembled structure and creates periodic structures similar to those of a Bragg reflector composed of high refractive and low refractive index layers. As shown in the light transmission curve in Figure 4a, the periodic internal structure has a photonic band gap at a wavelength of ca. 630 nm. It should be noted that blue emissive QDs do not have any absorption peak at wavelengths above 500 nm (see Supporting Information, Figure S2). In the case of free-standing $(PS-N_3)_{40}$ multilayers without QDs, the photonic band gap was not observed in the visible range (see Supporting Information, Figure

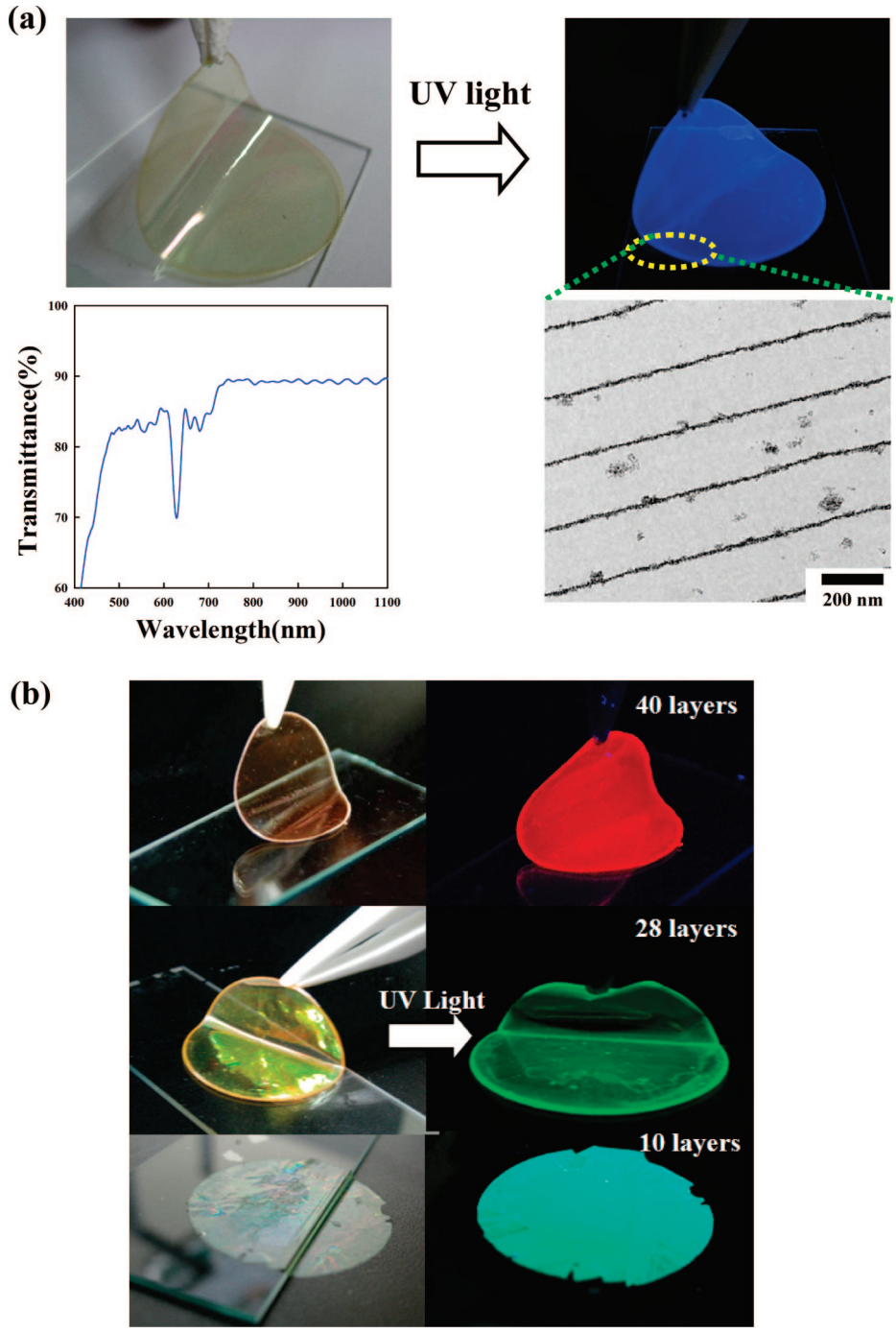

Figure 4. (a) Photographic images of free-standing multilayer films composed of $(PS-N_3{:}PS-N_3-SH\text{-stabilized blue QDs})_{40}$ multilayers before and after UV irradiation ($\lambda \approx 365$ nm). These images were taken with a digital camera. For the preparation of free-standing films, the multilayers were consecutively spin-deposited onto NaCl substrate and then separated by dissolving the substrate in a water bath. The internal structure and light transmission curve of free-standing multilayers were measured from cross-sectional TEM and UV−visible spectroscopy. (b) Photographic images of highly flexible free-standing $(PS-N_3-SH\text{-stabilized QDs:}PS-N_3)_n$ containing red emissive QDs ($n = 40$, film thickness $\sim 9 \pm 1$ μm), green emissive QDs ($n = 28$, film thickness $\sim 6 \pm 1$ μm), and blue-green emissive QDs ($n = 10$, film thickness ~ 3 μm). In this case, 40, 28, and 10 layered multilayers were spin-deposited at 3000, 3000, and 1500 rpm, respectively.

S5). The ability to have the polymer-coated nanoparticles segregate near the surface during spin-coating,[20] as schematically shown in Figure 5a, allows the internal structure of the multilayers to be further fine-tuned. As shown in Figure 5b, the presence of polymer (43 wt % $PS-N_3$) induces organic/inorganic multilayers with a stratified layer structure due to segregation of the $PS-N_3-SH-QDs$. Decreasing the relative amount of polymer, 15 wt % $PS-N_3-SH$, leads to an increase in the thickness of inorganic layer (Figure 5c), which allows the respective layer thicknesses to be easily tuned by the relative amount of polymers and nanoparticles. When the multilayer was prepared without any polymers, the QDs were evenly distributed within multilayers as shown in Figure 5d. Significantly, the $(PS-N_3-SH-QD{:}PS-N_3)_{28}$ multilayers in Figure 5b have the optical property of one-dimensional photonic crystals (see Supporting Information, Figure S6). From a practical viewpoint, the homogeneous distribution of nanoparticles is very important in electronic devices. For example, the semiconducting or metal

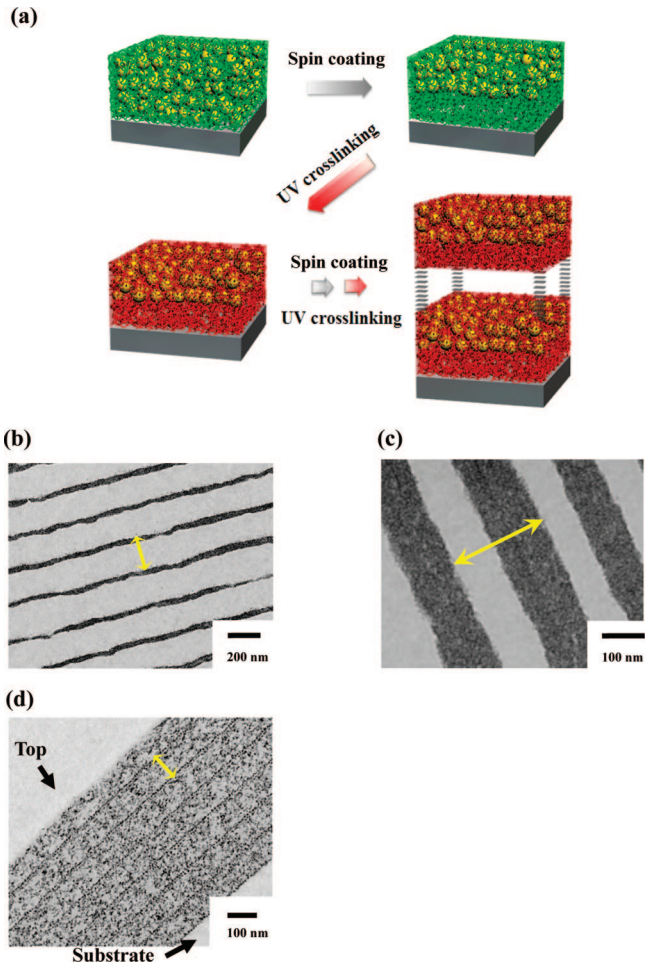

Figure 5. (a) Schematic for the buildup of $(PS-N_3-SH-QDs:PS-N_3)_n$ multilayers. Cross-sectional TEM images of (b) $(PS-N_3-SH-QDs:PS-N_3)_{28}$, (c) $(PS-N_3-SH-QDs)_{10}$ multilayers containing excess $PS-N_3-SH$ and (d) $(PS-N_3-SH-QDs)_7$ multilayers without excess $PS-N_3-SH$. As indicated by arrows, the single layer thicknesses of $(PS-N_3-SH-QDs:PS-N_3)_{28}$, $(PS-N_3-SH-QDs)_{10}$, and $(PS-N_3-SH-QDs)_7$ multilayers spin-deposited at 3000, 1500, and 1500 rpm are 265, 225, and 127 nm, respectively.

nanoparticles used for charge trap elements (i.e., data storage elements) in nonvolatile memory devices should be evenly dispersed and isolated within the insulating matrix.[8] Furthermore, considering that the classical LbL approach based on complementary interactions only allows the separate deposition of the respective layers (i.e., organic and inorganic layers) and the limited layer thickness (<10 nm), it should be noted that our approach provides the facile and versatile control of internal structure.

The ability to induce cross-linking by irradiation also suggests that the free-standing films can be patterned via a photolithographic process. As graphically illustrated in Figure 6a, patterned structures with a feature size of 500 μm could be prepared with free-standing multilayers. First, $PS-N_3$ multilayers were deposited onto a NaCl substrate through repetitive spin-coating and photocross-linking. Then, the $PS-N_3-SH-QD$ layer (2 wt % solution concentration) is spin-coated on the $(PS-N_3)_{30}$ multilayers followed by photocross-linked using a patterned shadow mask, and then the NaCl substrate is removed. As shown in Figure 6b, the resulting patterned free-standing multilayer exhibits highly photoluminescent properties. It should be also highlighted that various metal particles other than QDs can also

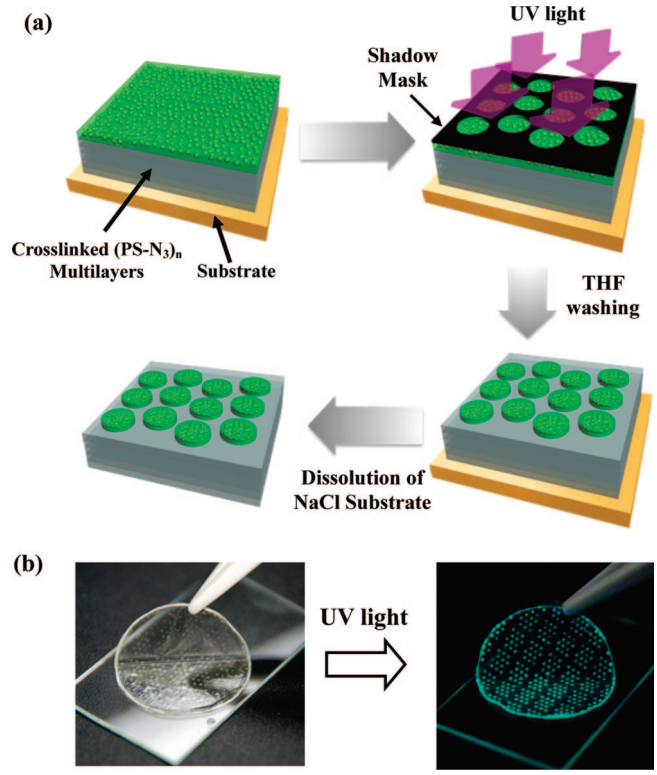

Figure 6. (a) Schematic for the preparation of patterned free-standing multilayer films. (b) Photographic images of $PS-N_3-SH-$green QD layer patterned onto $(PS-N_3)_{40}$ multilayer film. In this case, the size of the patterned dot is about 500 μm.

be incorporated into the patterned free-standing multilayers. For example, the thiol groups in $PS-N_3-SH$ can effectively stabilize Pt or Au nanoparticles[35−37] (see Supporting Information, Figure S7) and then be used to form free-standing organic−metal nanoparticle multilayers based on $PS-N_3-SH-Pt_{NP}$ or $PS-N_3-SH-Au_{NP}$ using the same method as for the QD-based multilayers. These patterned free-standing multilayers using ionic sacrificial substrates open up new possibilities in the design of advanced display panels or flexible electronics.

Conclusions

We have demonstrated a robust and efficient strategy for the fabrication of various organic−inorganic multilayers that allows for accurate control of individual layer thickness, internal structure, and nature of the inorganic nanoparticles. The key feature is the use of photocross-linkable polymers, $PS-N_3$ and $PS-N_3-SH$, which allows subsequent photolithographic patterning. The $PS-N_3-SH$ was used to modify the surface of nanoparticles (QD, Pt, and Au) and when mixed with a reactive matrix polymer $PS-N_3$ allows the construction of multilayers based on a repetitive spin-coating and UV cross-linking sequence. The thickness of individual layers within multilayers could be controlled from a few to hundreds of nanometers by varying the solution concentration and spinning speed. For nanocomposite multilayers based on polymers and polymer-coated QDs, enhanced photoluminescent durability was observed which allows for facile color tuning of the films according to the design of layer sequences. In addition, by adjusting the blending ratio of polymers and polymer-coated nanoparticles, self-assembly within the individual layers can be controlled leading to multilayer films which function as one-dimensional photonic crystals. These films open up new possibilities for the

fabrication of nanoscale devices for use in highly flexible optical or electronic applications such as display panels, nonvolatile memory, or organic thin film transistors. A key feature of this work is the robust, efficient, and versatile nature of this process for the preparation of smart nanocomposite multilayers.

Acknowledgment. This work was supported by the KOSEF grant funded by the Korea government (MEST) (R01-2008-000-10551-0), the "SystemIC2010" project of Korea Ministry of Commerce Industry and Energy (10030559), the ERC Program of KOSEF grant funded by the Korea government (MEST) (R11-2005-048-00000-0), and the Materials Research Laboratory (NSF DMR-0520415) at the University of California, Santa Barbara. We thank Frank Caruso for helpful suggestions and discussions.

Supporting Information Available: Photographic and TEM images of oleic acid- and PS−N_3−SH-stabilized QDs; NMR data of PS−N_3−SH-stabilized QD; PL stability; light transmission curve of free-standing films; 1D-photonic crystal films; free-standing films containing Au_{NP} and Pt_{NP}. This information is available free of charge via the Internet at http://pubs.acs.org/.

JA8064478

(36) Gittins, D. I.; Caruso, F. *Angew. Chem., Int. Ed. Engl.* **2001**, *40*, 3001–3004.

(37) Mayya, K. S.; Caruso, F. *Langmuir* **2003**, *19*, 6987–6993.